Elastography

Stéphane G. Carlier[a], Chris L. de Korte[b], Elisabeth Brusseau[b], Johannes A. Schaar[b], Patrick W. Serruys[c] and Anton F.W. van der Steen[b,d]

Intravascular ultrasound elastography is a method for measuring the local elastic properties of coronary atherosclerotic plaques using intravascular ultrasound (IVUS). Mechanical properties of the different tissues within a plaque are measured through strain. In the last decade, several groups have applied elastography intravascularly with various levels of success. In this paper, the approaches of the different research groups will be discussed and the focus will be on our approach to the application of intravascular elastography. *J Cardiovasc Risk* **9**: 1–9 © 2002 Lippincott Williams & Wilkins.

Journal of Cardiovascular Risk 2002, **9**: 1–9

Keywords: arteriosclerosis, ultrasonography, stress, mechanical

[a]Cardiovascular Centre, OLV Hospital, Aalst, Belgium, [b]Experimental Echocardiography Laboratory, Erasmus University, Rotterdam, [c]Thoraxcenter, Department of Interventional Cardiology, Erasmus Medical Center Rotterdam, Rotterdam, Heart Center and

Correspondence and requests for reprints to S.G. Carlier, PhD, Cardiovascular Centre Aalst, OLV hospital, Moorselbaan 164, B9300 Aalst, Belgium.
Tel: +3253724439; fax: +3253724185;
e-mail: stephane.carlier@OLVZ-aalst.be

Introduction

Sudden death is the leading symptom of coronary heart diseases in early middle age and stands at the most dreadful end of the spectrum of acute coronary syndromes. More than 50% of sudden deaths are related to an atherosclerotic plaque rupture or ulceration triggering thrombus formation and coronary occlusion [1,2]. Acute myocardial infarction and unstable angina are also related to a similar mechanism. A coronary atherosclerotic lesion can evolve over several years without any clinical symptom and flow limitation [3,4] Acute coronary syndromes frequently develop in arterial segments demonstrating only a mild stenosis on available prior angiograms [5,6] The plaque morphology, its composition and the importance of the infiltration of macrophages and lymphocytes, more than the degree of stenosis, are the determinants of acute clinical events [2,7–9] One of the major limitations of coronary angiography, the gold standard for the evaluation of symptomatic patients with coronary artery disease, is the inability to visualize the arterial wall [10]. Several techniques have been developed and are under development to characterize coronary atherosclerotic plaques [11]. The life-threatening plaques, prone to rupture, have been characterized by three major characteristics: (1) the size and structure of the atheromatous lipid core, (2) the thickness of the fibrous cap ($< 65\,\mu m$) and (3) the inflammation within or adjacent to the fibrous cap.

Catheter-based IntraVascular UltraSound (IVUS) is the only clinically available technique capable of providing real-time cross-sectional images of arteries *in vivo* [12,13]. IVUS provides quantitative information on the plaque burden and the lumen, as well as qualitative information on the plaque composition that has been compared with histology [14,15]. However, identification of the different plaque components is still limited: hard fibrous and soft plaques can show similar echo texture [16,17]. In particular, the sensitivity to identify lipid pools remains low [15]. Several IVUS-based methodologies have been proposed to improve tissue characterization [18–20] and detect plaque vulnerability [21,22]. However, IVUS, as well as other methodologies that have been developed [11] to detect rupture-prone plaques, are limited since they are based on the measurement of indirect vulnerability parameters such as plaque geometry, content, colour or

temperature. Plaque vulnerability is mainly a mechanical phenomenon: using computer simulations, concentrations of circumferential tensile stress were more frequently found in unstable plaques than in stable plaques [23,24]. For example, a thin fibrous cap shielding a lipid core from the blood may rupture since it is unable to bear the high circumferential stress due to the pulsating blood pressure (mechanical fatigue). These high-stress regions can be caused by the geometry of the plaque [25] or by local weakening of the plaque due to macrophage infiltration [26].

In 1991, a new technique was proposed directly to measure mechanical properties of tissue by ultrasound called elastography [27]. This technique has emerged to improve tissue characterization since a close correlation has been observed between the modification of the elastic properties of a tissue and the development of pathological processes. For example, it has been shown that the Young's modulus [28] (the ratio of a given force applied (stress) and the resulting deformation (strain)) of normal breast tissue is 20–40 kPa, but raises up to $>$ 500 kPa in breast carcinoma [29]. Elastography was developed using phantom studies [30] and evaluated *in vivo* [31]. The underlying principle is that a force (stress) is applied on the tissue and that the resulting strain is a function of the local mechanical properties [28]. The local strain of the material is obtained by means of comparing several ultrasound images acquired at different stress levels. Currently, this technique is developed in our laboratory for intravascular purposes. The objective of this paper is to give a short overview of different implementations of elastography. Next, the methods and results of our intravascular elastography work will be presented and discussed.

Previous related work

Several techniques have been proposed to study the mechanical properties of soft tissues using ultrasound. The main differences are in the type of mechanical solicitation of the tissue (vibration at low or high frequency, or quasi static compression) and in the signal processing methods used for estimating the local elastic properties.

Sonoelasticity: vibration amplitude imaging

Lerner and Parker presented preliminary work on vibration amplitude 'sonoelasticity imaging' [32]. With this method, a low-frequency vibration (20–500 Hz) is applied externally to excite internal vibrations within the tissue under study. A stiff inhomogeneity surrounded by soft tissue produces a disturbance in the normal vibration eigenmode patterns. Doppler detection techniques are employed to make a real-time vibration image. In some organs, modal patterns can be created, revealing additional information to the shear wave speed of sound of tissue [33]. Two real-time methods, static strain imaging and vibrography (using 0.1–20 Hz compressions) have been recently tested in phantom experiments. Real-time performance with a PC is achieved thanks to an original algorithm (phased root-seeking technique) to estimate the strain, faster than the cross-correlation methods [34].

Recently, Sandrin *et al.* have reported the results obtained in phantoms of a new method based on such a low-frequency shear wave (200 Hz) visualized by means of an ultrafast imaging system (up to 10 000 frames/s) composed of a linear array of transducers at 3.5 MHz [35]. Sonoelasticity has not been evaluated for vascular tissue, but given the large wavelengths and the level of inhomogeneity in a diseased vessel, it seems not to be the technique of first choice. Ongoing research investigates the feasibility to use magnetic resonance elastography using propagating acoustic shear waves [36,37].

kHz dynamics: vibration amplitude imaging

In this technique, the tissue is excited using a 15–25 kHz sound field and the amplitude of vibration is measured with a 30 MHz transducer [38]. The amplitude of compression waves is related to the mechanical properties of the tissue but also on the size of the tissue inhomogeneities and resonance phenomena. Because of the potential problems related to the *in vivo* intravascular application of a 20 kHz sound field, this approach has been abandoned for intravascular elasticity imaging.

Ultrasound-stimulated vibro-acoustic spectrography

Fatemi and Greenleaf have proposed an alternative method based on the acoustic energy emitted from solids and tissue in response to an oscillatory radiation force produced by interfering focused beams of ultrasound. Interference in the intersection region of the two beams produces sinusoidal modulation of the ultrasound energy density that creates an oscillatory force vibrating the object at the selected region that can be measured some distance away. Using two coaxial, confocal transducer elements of a spherically focused annular array, they could image excised human iliac arteries and clearly detect calcified regions [39].

Elastography: compression strain imaging

Elastography is an imaging technique based on the static deformation of a linear isotropic elastic material. The tissue under inspection is externally compressed and the displacement between pairs of A-lines with and without compression is determined using cross-correlation analysis [27,30]. From these data, the strain profile in the tissue under study can be determined. Whereas Ophir *et al.* did not explore intravascular application, our group has demonstrated the feasibility of performing *in vivo* coronary elastography. The compression can be obtained from the systemic pressure difference or by using a compliant intravascular balloon [40]. The following techniques are all more or less based on this excitation principle, but use a variety of detection methods.

Envelope based intravascular elastography Ryan and Foster developed a technique based on comparison of pre- and postcompression of vessel mimicking phantoms [41]. The displacement in these phantoms was based on speckle tracking in the video signals. The strain is calculated from this displacement. It was shown that phantom components of different hardness had different displacement magnitude. For use under physiological circumstances, the method still needs quite some adaptation. A big advantage of using the envelope is the fact that the correlation function is smoother than the RF-based correlation function and that the video signal is commonly available from any commercial echosystem. The disadvantage is the limited resolution. For intravascular applications, small tissue strains must be measured and therefore the use of RF data dramatically improves the resolution.

Spectral tissue strain Talhami *et al.* introduced a technique that is capable of estimating the global radial strain in a vessel [42]. The technique is based on the Fourier scaling property of the signals and uses the chirp Z-transform. The envelope data are used for this analysis. The result is displayed as a colour-coded ring around the image of the vessel. Initial results on vascular tissue *in vitro* and *in vivo* have been described, but without a validation of the technique.

Phase sensitive speckle tracking multicompression elasticity imaging Shapo *et al.* developed another technique that is based on cross-correlation of A-lines [43,44]. This group proposed a large deformation to maximize the signal-to-noise ratio of the displacement and strain estimation. However, a large displacement will decorrelate the ultrasound signals to such an extent that correlation detection is unreliable. For this reason, the cross-correlation is calculated in several intermediate steps of intraluminal pressure. For detection, they use a phase-sensitive speckle tracking technique. The technique uses an IVUS catheter that is inserted in a compliant balloon. The balloon is used to strain the tissue up to 40%. The feasibility of this technique was demonstrated in simulations and tissue mimicking phantoms. Currently the technique is validated *in vitro*.

Broad-band radiofrequency-based elastography Radiofrequency data are acquired at two levels of intraluminal pressure. The estimation of the deformation remains, in general, a study of the correlation between signals acquired before and after the application of a stress. The most common signal-processing technique used in elastography considers the local displacements within soft biological tissues as simple translations. Within the RF signal, these displacements will be translated by a delay of the acoustical signatures of the respective tissue regions. This results in a modelling of the postcompression signal as a locally delayed replica of the predeformation signal. The local tissue displacement is, in this case, a simple shift. It is computed as the location of the maximum of the cross-correlation function of gated pre- and postcompression echo signals (*time-delay estimation*). The strain is then computed as the displacement derivative [45,46]. In the case of small deformations [0–2%], these techniques have proved to be efficient and accurate. However, they fail rapidly with increasing strains since then the signal is subjected to a variation in shape that has not been taken into account.

Another approach taking into account the change in shape of the signals has been recently described (*local scaling factor estimation*) [47–49]. The signal after compression is processed as a delayed and scaled replica of the signal before deformation. These methods have been shown to be more robust to large deformation, but the performance for small strain values ($< 2\%$) remains low. An adaptative strain estimation method based on the computation of local scaling factors has been successfully applied to compute elastograms of cryogel phantoms mimicking vessels and of a freshly excised human carotid artery using a 30 MHz mechanical rotating single element ultrasound scanner (ClearView, CVIS, Boston Scientific Corp.) [50].

We will focus the rest of this review on the intravascular elastography methods that have been developed in our laboratory. Data are acquired at two levels of intraluminal pressure. Displacement and

strain are calculated from broadband RF traces. The strain information is presented as an independent complementary two-dimensional image of the echogram when it has been computed across the complete vessel wall (elastogram) or as one-dimensional colour-coded line congruent with the lumen perimeter when the strain is computed only for the inner layer of the arterial wall (palpogram) [51].

Materials and methods

Materials

Phantom Vessel phantoms with the morphology of atherosclerotic vessels were constructed from solutions of agar and gelatin with carborundum (SiC) particles used for scattering. A hard vessel containing a soft lesion with no echogenicity contrast between the wall and plaque was measured with intraluminal pressures of 50 and 55 mmHg [52].

Femoral and coronary arteries in vitro Atherosclerotic human femoral ($n = 10$) and coronary ($n = 4$) arteries obtained postmortem were measured *in vitro*. Two IVUS scans were acquired at 80 mmHg and 100 mmHg. The vessel specimens were then fixed in a buffered formaldehyde solution (3.6%) and processed for routine paraffin embedding. For each segment, cross-sections were stained for collagen (picro-Sirius red stain), for smooth muscle cells (anti-α-actin stain) and for macrophages (anti-CD68 stain) [53].

Coronary arteries in vivo Data were obtained from patients ($n = 12$) referred for percutaneous coronary intervention. After intravenous administration of heparin and acetylsalicylic acid, a 6-Fr guiding catheter was advanced up to the ostium of the involved artery. After coronary injection of a bolus of 3 mg isosorbide dinitrate, preintervention IVUS assessment of the lesion was performed [54].

The acquisition and signal processing have been explained in detail elsewhere [55] and are beyond the scope of this review. In summary, *in vitro* experiments on human femoral arteries were performed with a 4.3F Princeps® 30-MHz catheter (Dumed) connected to a stepper motor. The *in vitro* and *in vivo* coronary recordings were performed using a 64-F/X array IVUS transducer (EndoSonics/JoMed). *In vivo*, lesions were crossed and imaged without complication. The pressure was measured at the level of the coronary ostium via the guiding catheter connected to a standard fluid-line system. Ten microseconds ($\sim$7.5 mm) of the 64 angles (in Chromaflow mode) analogue RF data output of the InVision system were digitized at high frequency (200 MHz, in 8 bits). Ten frames per second were acquired at cross-sections where the IVUS echogram revealed diseased vessel wall and plaque. Due to the contraction of the heart, the catheter is moving in the lumen. For large motions, the frames acquired at the different intraluminal pressures may be misaligned thus hindering adequate displacement estimates. An algorithm to determine the similarity between sequential echo frames has been used as a figure of merit for the motion of the catheter in the lumen. Sequential frames with a high likelihood and a pressure differential large enough to result in strain levels of the order of 1% were processed to derive the elastograms.

Results

The principle of intravascular elastography is visualized in Figures 1 and 2: the echo signal of the soft region (light grey) shows minute changes once the applied force has compressed this tissue, whereas the signal from the hard region (dark grey) remains nearly identical since the tissue thickness in that region did not change. Figure 2 shows the echogram of the phantom acquired at low pressure is in the upper left corner. The echogram acquired at high pressure is shown in the lower left corner. The soft plaque area is not visible in the echograms. The local strain determined using the cross-correlation based time delay estimation algorithm is shown on the right. The soft plaque region is clearly visible in the elastogram from 7 to 11 o'clock.

An echogram, elastogram and histology of a human femoral artery segment are shown in Figure 2. The echogram of this artery shows a slightly eccentric plaque with different echogenicities. Although the echogram perfectly reveals the geometry of this plaque, its composition remains uncertain. The elastogram reveals that the plaque can be divided into four quadrants: (a) and (c) demonstrating a low-compressibility, (b) and (d) with a higher compressibility. The strain in the low-compressing parts (0.2%) indicates that this may be fibrous tissue, which was confirmed by histology. The histology of the regions with a higher strain values (0.8–1%) reveals fatty material with macrophage accumulation. At each location investigated ($n = 45$), 2 IVUS images were acquired at different intraluminal pressures (80 and 100 mmHg). Elastographic data and histology were matched using the IVUS echogram. The cross-sections

Fig. 1

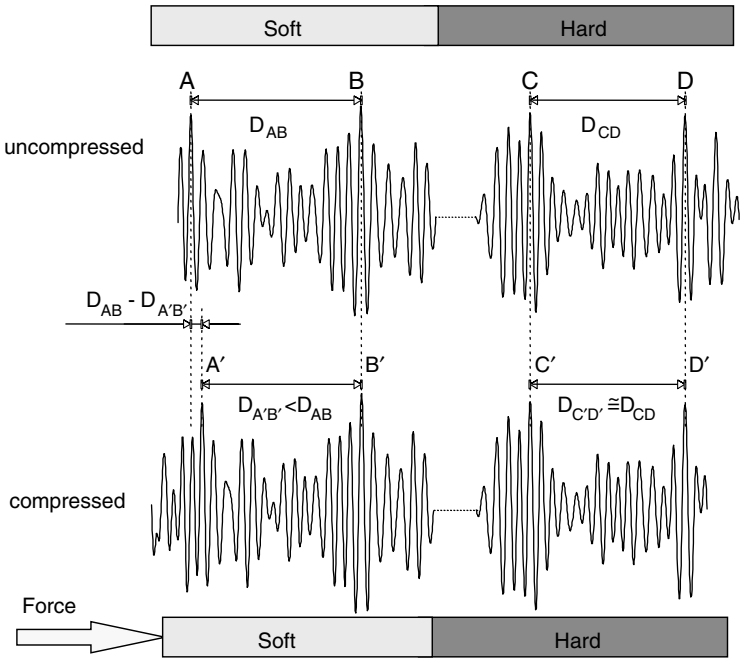

Principle of elastography: the echo signals of a soft material (left panel) show minute deformation once the material is compressed by the applied force. The distance D_{AB}, which can be measured by estimation of temporal shifts in the radiofrequency signal, is decreased to $D_{A'B'}$. On the contrary, with the absence of compression of the hard material (right panel), there is no change in the radiofrequency signal and $D_{CD} \sim = D_{C'D'}$.

Fig. 2

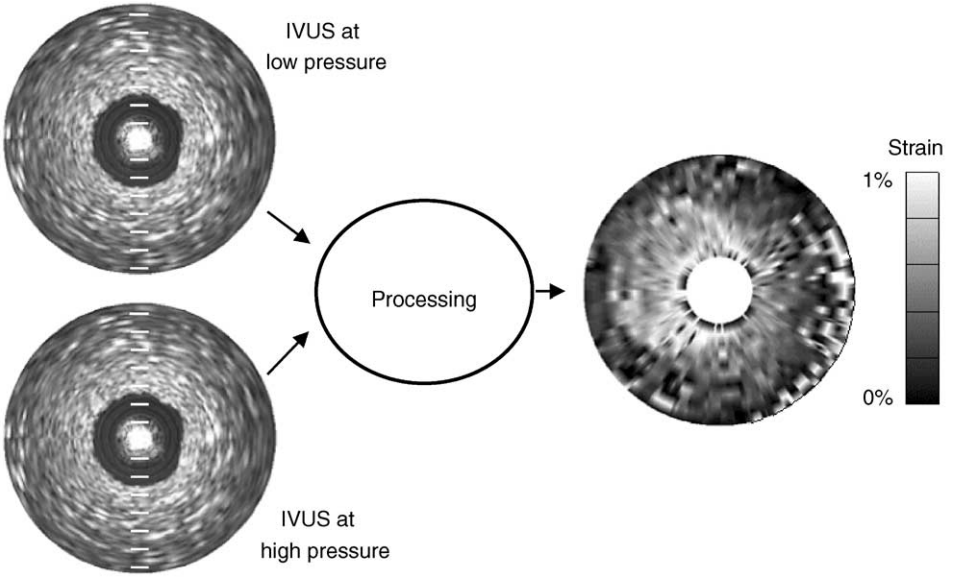

Schematic representation of deriving elastograms. From 2 IVUS images acquired at low (upper panel) and high pressure (lower panel), no detection of the soft inclusion in this phantom is possible. However, using cross-correlation techniques, the local strain can be measured and plotted as an additional image on the right, showing the softer region between 7 and 11 o'clock demonstrating a higher strain.

were segmented in regions ($n = 125$) that were based on the strain values on the elastogram. The dominant plaque types in these regions (fibrous, fibro-fatty, or fatty) were obtained from histology and correlated with the average strain and echo intensity. The strain for the three plaque types as determined by histology differed

Fig. 3

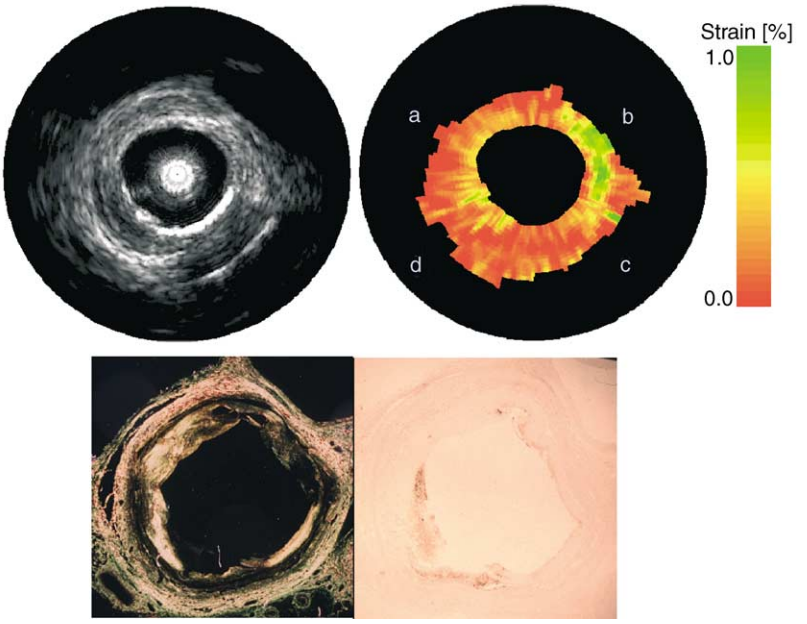

Intravascular echogram (top left) and elastogram (top right) of a diseased human femoral artery with corresponding histology: bottom left, picro-Sirius red with polarized light microscopy (for collagen staining), bottom right, anti-CD68 antibody (for macrophage staining). Echogram shows a slightly eccentric plaque with different echogenicities. Elastogram reveals two soft regions (b and d) and two harder regions (a and c). Histology reveals that the soft regions b and d contain mainly fatty material and shows macrophage accumulation in d.

Fig. 4

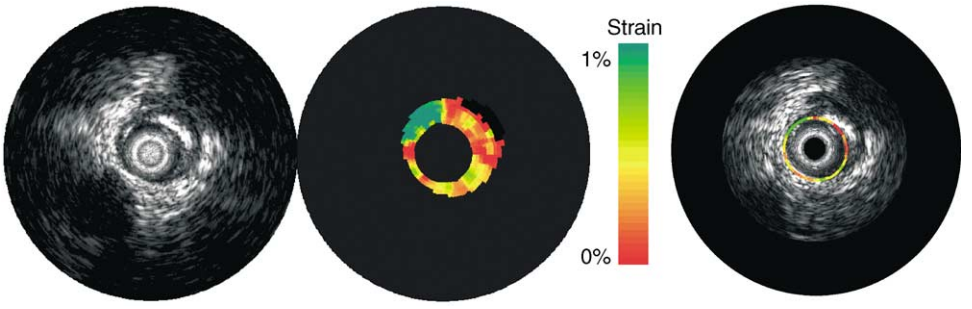

In vivo echogram (left panel), elastogram (centre) and palpogram (right panel) of a cross section in the left anterior descending artery of a patient. The echogram reveals calcified material between noon and 3 o'clock. In this region, a very low strain value was assessed on both the elastogram and the palpogram (colour-coded in red).

significantly ($P = 0.0002$). This difference was mainly evident between fibrous and fatty tissue ($P = 0.0004$). The plaque types did not reveal echo-intensity differences in the IVUS echogram ($P = 0.882$) [53].

In all *in vivo* experiments, elastograms were determined from two echograms acquired near end-diastole. Analysis of the likelihood curves revealed that the minimal motion of the catheter was present in this part of the heart cycle for all patients. There was on average a pressure differential of approximately 5 mmHg between sequential frames in this part of the heart cycle. Figure 4 demonstrates an echogram, an elastogram and a palpogram of a human coronary artery. The echogram reveals a large calcified area (from noon to 3 o'clock). The elastogram and the palpogram identify this area as being composed of hard material since low strain values are found in this region. Among the 12 patients investigated, three demonstrated similar calcified regions ($104 \pm 70^{\circ}$). The corresponding average strain was 0.20 ± 0.07. Conversely, the average strain in all noncalcified regions was 0.51 ± 0.20 ($P < 0.001$).

Discussion

Imaging tissue elastic parameters is rapidly drawing attention for its ability to provide new information on biological tissue. Intravascular elastography has been developed to assess the local mechanical properties of the vascular wall. Knowledge of the mechanical properties may help the clinician in choosing the proper interventional technique and in detecting rupture prone plaques.

The phantom experiments demonstrate that hard and soft material can be identified by IVUS elastography, independently of the echogenicity contrast of the materials.

The results of the *in vitro* experiments on human femoral arteries support these findings. Fibrous material was identified by the low strain values as observed from the elastogram. In the specimen containing two plaque types, the elastogram clearly revealed the fibrous and the fatty plaque region. This identification was not possible using the echogram since both regions demonstrated the same echogenicity.

These findings make the technique promising for the identification of rupture-prone plaques characterized by a necrotic core and a thin, fibrous cap [2]. The rupture of a plaque often occurs at places with a high stress concentration [56]. The elastogram does not provide information on the source of this high-strain region that can be caused by soft material present in this region or by a stress concentration caused by the geometry. Figure 3 shows that, in this particular case, the high radial strain was related to the accumulation of fatty material. Additionally, an increased macrophage concentration has been observed in regions with high strain values. The sensitivity and specificity of the technique remain to be investigated to identify different plaque components and vulnerable regions.

For *in vivo* elastograms of diseased human coronary arteries, a dynamic instead of static pressure differential is used to strain the tissue. The advantage is that this excitation source is naturally present in the arterial system. Using gated acquisition, different levels of intravascular pressure are obtained. Our preliminary results indicate that reproducible elastograms and palpograms can be obtained with this acquisition set-up scheme. The elastographic findings could not be validated using histology during the *in vivo* experiments. Therefore, only a partial validation has been performed using the low resolution echogram (64 angles of the Chromaflo imaging mode) to differentiate between calcified and noncalcified material. Since echography gives no information regarding the presence of lipid or fibrous material, further validation has not been possible at this point. A dramatic improvement in the RF signal acquisition scheme has been obtained recently with a direct digital interface incorporated in the Endosonics In-Vision console that communicates directly with a PC in which long sequences of RF echo frames at full rate can be stored in random access memory. High-resolution IVUS images (12 bits resolution, 512 phased-array angles) are now available for comparison with the elastograms.

Compared with the *in vitro* experiments on human femoral arteries, the pressure differential between the two frames is smaller: 3–5 mmHg instead of 20 mmHg. A smaller pressure differential will immediately result in lower strain values. However, the strain values found during the *in vivo* experiments are in the same range as those found in the *in vitro* experiments indicating that the tissue during *in vivo* examination is softer. A possible explanation is that the elastic moduli of tissue will be elevated after excision of the tissue [57] and may even increase further after cold storage. Additionally, since the *in vitro* study was performed at room temperature, fatty tissues will be harder at room temperature than at body temperature resulting in decreased strain values.

One of the limitations of intravascular elastography at present is the computing time required and the use of only one-dimensional echo-tracking. Elastographic methods to compute both lateral and axial strains have been reported recently [58]. The palpograms have been developed in order to improve the clinical applicability and the robustness in presence of catheter movements *in vivo* as well as to advance coronary elasticity to real-time imaging [51]. This technique produces compound images of the strain obtained of the first part of the arterial wall (user defined, typical 600 μm) and conventional sonographic information. Palpograms are computed by applying a two-dimensional echo-tracking technique, an outlier rejection filter and a finite difference strain estimator. A composite palpogram, as illustrated in Figure 4 (right panel), reconstructed for each cardiac cycle of a 6-s acquisition can currently be computed in less than a minute [59].

A final limitation of intravascular elastography to stress is that so far we have computed maps of the strain inside the arterial wall, but not of Young's modulus. Theoretically, the reconstruction of Young's modulus

would improve the accuracy of tissue characterization and would be independent of the local stress magnitude and its inhomogeneous distribution. This final step in elasticity imaging has been described for nonvascular applications [58,60], but is still under preliminary investigation in our laboratory.

Conclusion

Intravascular elastography encompasses techniques based on conventional IVUS providing a means for remote palpation and elasticity quantitation of the vessel wall. We have obtained the first elastograms of diseased arteries *in vitro* and *in vivo*. The results show that tissue characterization based on elasticity information from regions with various pathologies may be feasible. This method could potentially improve the detection of rupture-prone plaque based on the assessment of locally increased strain. This information, which is useful for diagnosis and guiding interventional procedures, is frequently inconclusive or unavailable from IVUS echograms or X-ray angiograms.

Acknowledgements

The authors thank EI Cespedes (JoMed imaging, Rancho Cordova, CA) for his critical comments on this review and his endeavours to bring intravascular elastography to clinical practice.

References

1 Davies MJ, Thomas AC. Plaque fissuring – the cause of acute myocardial infarction, sudden ischaemic death, and crescendo angina. *Br Heart J* 1985; **53(4)**:363–373.

2 Virmani R, Kolodgie FD, Burke AP, Farb A, Schwartz SM. Lessons from sudden coronary death: a comprehensive morphological classification scheme for atherosclerotic lesions. *Arterioscler Thromb Vasc Biol* 2000; **20(5)**:1262–1275.*
The introduction of a simplified classification, in comparison to the AHA classification (Ref. 7), that is based on descriptive morphology of atherosclerotic lesions, extensively illustrated with numerous histological examples of high educational quality.

3 Glagov S, Weisenberg E, Zarins CK. Compensatory enlargement of human atherosclerotic coronary arteries. *N Engl J Med* 1987; **316**:1371–1375.

4 Ge J, Erbel R, Gerber T, Gorge G, Koch L, Haude M, *et al.* Intravascular ultrasound imaging of angiographically normal coronary arteries: a prospective study *in vivo*. *Br Heart J* 1994; **71(6)**:572–578.

5 Ambrose JA, Tannenbaum MA, Alexopoulos D, Hjemdahl-Monsen CE, Leavy J, Weiss M, *et al.* Angiographic progression of coronary artery disease and the development of myocardial infarction. *J Am Coll Cardiol* 1988; **12(1)**:56–62.

6 Little WC, Constantinescu M, Applegate RJ, Kutcher MA, Burrows MT, Kahl FR, *et al.* Can coronary angiography predict the site of a subsequent myocardial infarction in patients with mild-to-moderate coronary artery disease? *Circulation* 1988; **78(5 Pt 1)**:1157–1166.

7 Stary HC, Chandler AB, Dinsmore RE, Fuster V, Glagov S, Insull W Jr., *et al.* A definition of advanced types of atherosclerotic lesions and a histological classification of atherosclerosis. A report from the Committee on Vascular Lesions of the Council on Arteriosclerosis, American Heart Association. *Circulation* 1995; **92(5)**:1355–1374.

8 Falk E, Shah PK, Fuster V. Coronary plaque disruption. *Circulation* 1995; **92(3)**:657–671.

9 van der Wal AC, Becker AE, van der Loos CM, Das PK. Site of intimal rupture or erosion of thrombosed coronary atherosclerotic plaques is characterized by an inflammatory process irrespective of the dominant plaque morphology. *Circulation* 1994; **89(1)**:36–44.

10 Topol EJ, Nissen SE. Our preoccupation with coronary luminology. The dissociation between clinical and angiographic findings in ischemic heart disease. *Circulation* 1995; **92**:2333–2342.

11 Pasterkamp G, Falk E, Woutman H, Borst C. Techniques characterizing the coronary atherosclerotic plaque: influence on clinical decision making? *J Am Coll Cardiol* 2000; **36(1)**:13–21.*
An excellent introduction of the characteristics of rupture-prone plaques and a critical review of the imaging techniques developed to characterize atherosclerotic lesions. The respective clinical relevance of each method is discussed.

12 di Mario C, Görge G, Peters R, Kearney P, *et al.* Clinical application and image interpretation in intracoronary ultrasound. Study Group on Intracoronary Imaging of the Working Group of Coronary Circulation and of the Subgroup on Intravascular Ultrasound of the Working Group of Echocardiography of the European Society of Cardiology. *European Heart J* 1998; **19(2)**: 207–229.

13 Nissen S, Yock P. Intravascular ultrasound. Novel pathophysiological insights and current clinical applications. *Circulation* 2001; **103**:604–616.

14 di Mario C, The SHK, Madrestma S, van Suylen RJ, Wilson RA, Bom N, *et al.* Detection and characterization of vascular lesions by intravascular ultrasound: an *in vitro* study correlated with histology. *J Am Soc Echocardiography* 1992; **5(2)**:135–146.

15 Prati F, Arbustini E, Labellarte A, Dal Bello B, Sommariva L, Mallus MT, *et al.* Correlation between high frequency intravascular ultrasound and histomorphology in human coronary arteries. *Heart* 2001; **85(5)**:567–570.

16 Kimura BJ, Bhargava V, DeMaria AN. Value and limitations of intravascular ultrasound imaging in characterizing coronary atherosclerotic plaque. *Am Heart J* 1995; **130(2)**:386–396.

17 Hiro T, Leung CY, De Guzman S, Caiozzo VJ, Favid AR, Karimi H, *et al.* Are soft echoes really soft? Intravascular ultrasound assessment of mechanical properties in human atherosclerotic tissue. *Am Heart J* 1997; **133**:1–7.

18 Wilson LS, Neale ML, Talhami HE, Appleberg M. Preliminary results from attenuation-slope mapping of plaque using intravascular ultrasound. *Ultrasound in Med and Biol* 1994; **20(6)**:529–542.

19 Komiyama N, Berry GJ, Kolz ML, Oshima A, Metz JA, Preuss P, *et al.* Tissue characterization of atherosclerotic plaques by intravascular ultrasound radiofrequency signal analysis: An *in vitro* study of human coronary arteries. *Am Heart J* 2000; **140(4)**:565–574.

20 Vince DG, Dixon KJ, Cothren RM, Cornhill JF. Comparison of texture analysis methods for the characterization of coronary plaques in intravascular ultrasound images. *Comput Med Imaging Graph* 2000; **24(4)**:221–229.

21 Yamagishi M, Terashima M, Awano K, Kijima M, Nakatani S, Daikoku S, *et al.* Morphology of vulnerable coronary plaque: insights from follow-up of patients examined by intravascular ultrasound before an acute coronary syndrome. *J Am Coll Cardiol* 2000; **35(1)**:106–111.

22 Hiro T, Fujii T, Yasumoto K, Murata T, Murashige A, Matsuzaki M. Detection of fibrous cap in atherosclerotic plaque by intravascular ultrasound by use of color mapping of angle-dependent echo-intensity variation. *Circulation* 2001; **103(9)**:1206–1211.

23 Cheng GC, Loree HM, Kamm RD, Fishbein MC, Lee RT. Distribution of circumferential stress in ruptured and stable atherosclerotic lesions. A structural analysis with histopathological correlation. *Circulation* 1993; **87**:1179–1187.

24 Richardson PD, Davies MJ, Born GVR. Influence of plaque configuration and stress distribution on fissuring of coronary atherosclerotic plaques. *Lancet* 1989; **21**:941–944.

25 Loree HM, Kamm RD, Stringfellow RG, Lee RT. Effects of fibrous cap thickness on peak circumferential stress in model atherosclerotic vessels. *Circulation Res* 1992; **71**:850–858.

26 Lendon CL, Davies MJ, Born GVR, Richardson PD. Atherosclerotic plaque caps are locally weakened when macrophage density is increased. *Atherosclerosis* 1991; **87**:87–90.

27 Ophir J, Céspedes EI, Ponnekanti H, Yazdi Y, Li X. Elastography: a method for imaging the elasticity in biological tissues. *Ultrasonic Imaging* 1991; **13**:111–134.

28 Lee RT, Kamm RD. Vascular mechanics for the cardiologist. *J Am College of Cardiology* 1994; **23(6)**:1289–1295*
An extensive review of vascular mechanics introducing the terminology and basic principles of the relation of stress and strain. Methods to measure vessel wall stiffness are described in details.

29 Krouskop TA, Wheeler TM, Kallel F, Garra BS, Hall T. Elastic moduli of breast and prostate tissues under compression. *Ultrasonic Imaging* 1998; **20(4)**:260–274.

30 Céspedes EI. Elastography: imaging of biological tissue elasticity [PhD]. Houston, Texas, CA, USA: University of Houston; 1993.

31 Céspedes EI, Ophir J, Ponnekanti H, Maklad N. Elastography: elasticity imaging using ultrasound with application to muscle and breast *in vivo*. *Ultrasonic Imaging* 1993; **17**:73–88.

32 Lerner RM, Parker KJ. Sonoelasticity images, ultrasonic tissue characterization and echographic imaging. Paper presented at: 7th European Communities Workshop, 1987; Nijmegen, The Netherlands.

33 Parker KJ, Lerner RM. Sonoelasticity of organs, shear waves ring a bell. *J Ultrasound in Medicine* 1992; **11**:387–392.

34 Pesavento A, Lorenz A, Siebers S, Ermert H. New real-time strain imaging concepts using diagnostic ultrasound. *Phys Med Biol* 2000; **45**: 1423–1435.

35 Sandrin L, Catheline S, Tanter M, Hennequin X, Fink M. Time-resolved pulsed elastography with ultrafast ultrasonic imaging. *Ultrasonic Imaging* 1999; **21(4)**:259–272.

36 Muthupillai R, Lomas DJ, Rossman PJ, Greenleaf JF, Manduca A, Ehman RL. Magnetic resonance elastography by direct visualization of acoustic strain waves. *Science* 1995; **269**:1854–1857.

37 Kruse SA, Smith JA, Lawrence AJ, Dresner MA, Manduca A, Greenleaf JF, *et al.* Tissue characterization using magnetic resonance elastography: preliminary results. *Phys Med Biol* 2000; **45(6)**:1579–1590.

38 de Korte CL, Céspedes EI, van der Steen AFW, Lancée CT. Local compressibility assessment using 20 kHz sound excitation. *Ultrasonic Imaging* 1996; **18(2)**:67–68.

39 Fatemi M, Greenleaf JF. Ultrasound-stimulated vibro-acoustic spectrography. *Science* 1998; **280**:82–85.

40 Sarvazyan AP, Emelianov SY, Skovorada AR, inventors. Intracavity device for elasticity imaging. US patent 5,265,612, November 39. 1993.

41 Ryan LK, Foster FS. Ultrasonic measurement of differential displacement and strain in a vascular model. *Ultrasonic Imaging* 1997; **19**:19–38.

42 Talhami HE, Wilson LS, Neale ML. Spectral tissue strain: a new technique for imaging tissue strain using intravascular ultrasound. *Ultrasound Med Biol* 1994; **20(8)**:759–772.

43 Shapo BM, Crowe JR, Skovoroda AR, Eberle M, Cohn NA, O'Donnell M. Displacement and strain imaging of coronary arteries with intraluminal ultrasound. *IEEE Trans Ultrasonics, Ferroelectrics, and Frequency Control* 1996; **43(2)**:234–246.

44 Shapo BM, Crowe JR, Erkamp R, Emelianov SY, Eberle M, O'Donnell M. Strain imaging of coronary arteries with intraluminal ultrasound: experiments on an inhomogeneous phantom. *Ultrasonic Imaging* 1996; **18**:173–191.

45 Céspedes EI, de Korte CL, van der Steen AFW, von Birgelen C, Lancée CT. Intravascular elastography: principle and potentials. *Semin Interventional Cardiol* 1997; **2(1)**:55–62.

46 de Korte CL, van der Steen AF, Cespedes EI, Pasterkamp G. Intravascular ultrasound elastography in human arteries: initial experience *in vitro*. *Ultrasound Med Biol* 1998; **24(3)**:401–408.

47 Alam KS, Ophir J, Konofagou E. An adaptative strain estimator for elastography. *IEEE Trans Ultrasonics, Ferroelectrics, and Frequency Control* 1998; **45(2)**:461–472.

48 Bilgen M. Wavelet-based strain estimator for elastography. *IEEE Trans Ultrasonics, Ferroelectrics, and Frequency Control* 1999; **46(6)**:1407–1415.

49 Brusseau E, Perrey C, Delachartre P, Vogt M, Vray D, Ermert H. Axial strain imaging using a local estimation of the scaling factor from RF ultrasound signals. *Ultrasonic Imaging* 2000; **22(2)**:95–107.

50 Brusseau E, Fromageau J, Finet G, Delachartre P, Vray D. Axial strain imaging of intravascular data: results on polyvinyl alcohol cryogel phantoms and carotid artery. *Ultrasound Med Biol* 2001; **2**:1631–1642.

51 Cespedes EI, de Korte CL, van der Steen AF. Intraluminal ultrasonic palpation: assessment of local and cross- sectional tissue stiffness. *Ultrasound Med Biol* 2000; **26(3)**:385–396.

52 de Korte CL, Céspedes EI, van der Steen AFW, Lancée CT. Intravascular elasticity imaging using ultrasound: feasibility studies in phantoms. *Ultrasound Med Biol* 1997; **23(5)**:735–746.

53 de Korte CL, Pasterkamp G, van Der Steen AF, Woutman HA, Bom N. Characterization of plaque components with intravascular ultrasound elastography in human femoral and coronary arteries *in vitro*. *Circulation* 2000; **102(6)**:617–623.*
Description of the IVUS elastography methodology with the demonstration of a statistically significant difference between fibrous, fibrofatty and fatty plaque components. The potential of this new method to detect rupture-prone plaques characterized by macrophage concentration is also presented.

54 de Korte CL, Carlier SG, Mastik F, Doyley MM, van der Steen AFW, Serruys PW, *et al.* Morphologic and mechanic information of coronary arteries obtained with intravascular elastography: feasibility study *in vivo*. *Eur Heart J* 2002; **23**:405–131.**
The first clinical demonstration of the feasibility to perform IVUS elastography. Although no histological validation was possible in these patients planned for coronary angioplasty, this article will remain a cornerstone in the development of a mean for remote palpation and elasticity quantitation of the coronary vessel wall.

55 de Korte CL, van der Steen AF, Cepedes EI, Pasterkamp G, Carlier SG, Mastik F, *et al.*. Characterization of plaque components and vulnerability with intravascular ultrasound elastography. *Phys Med Biol* 2000; **45(6)**:1465–1475.

56 Lee RT, Loree HM, Cheng GC, Lieberman EH, Jaramillo N, Schoen FJ. Computational structural analysis based on intravascular ultrasound imaging before *in vitro* angioplasty: prediction of plaque fracture locations. *J Am College of Cardiology* 1993; **21**:777–782.

57 Gow BS, Hadfield CD. The elasticity of canine and human coronary arteries with reference to post-mortem changes. *Circulation Research* 1979; **45(5)**:588–594.

58 Konofagou E, Ophir J. A new elastographic method for estimation and imaging of lateral displacements, lateral strains, corrected axial strains and Poisson's ratios in tissues. *Ultrasound Med Biol* 1998; **24(8)**:1183–1199.

59 Doyley MM, de Korte CL, Mastik F, Carlier SG, Cespedes E, van der Steen AFW, *et al.* Clinical intravascular elasticity imaging: methods and performance evaluation. *Ultrasound Med Biol* 2001; **27**:1471–1480.

60 Emelianov SY, Lubinski MA, Skovoroda AR, Erkamp RQ, Leavey SF, Wiggins RC, *et al.* Reconstructive ultrasound elasticity imaging for renal transplant diagnosis: kidney ex vivo results. *Ultrasonic Imaging* 2000; **22(3)**:178–194.

AUTHOR QUERY FORM

LIPPINCOTT WILLIAMS AND WILKINS

JOURNAL TITLE: HJR DATE: 6/9/2002
ARTICLE NO. : 200203

Queries and / or remarks

Manuscript Page/line	Details required	Author's response
	No query	